Article ID: 1000-324X(2021)01-0095-06 **DOI:** 10.15541/jim20190564

Electron Irradiation Induced Phase-separation Behavior in AlF_3 Doped Alumina Ceramic with Superior Sensitivity

SHEN Lu[1], WANG Dewen[2], HUANG Rong[3], DU Shiyu[1], HUANG Qing[1]

(1. Ningbo Institute of Materials Technology and Engineering, Chinese Academy of Sciences, Ningbo 315201, China; 2. Shanghai Institute of Ceramics, Chinese Academy of Sciences, Shanghai 200050, China; 3. Key Laboratory of Polar Materials and Devices (MOE), Department of Electronics, East China Normal University, Shanghai 200062, China)

Abstract: An electron irradiation induced fast phase-separation behavior was observed under convention Transmission electron microscopy (TEM) observation of spark plasma sintered AlF_3 doped alumina ceramic. Spherical nanocrystalline Al precipitates separated out from original alumina grain surface within several seconds under transmission electron microscopy electron irradiation. By high resolution TEM observation combined with diffraction patterns analysis, it was found that the original alumina grain surface was in highly defected state. After electron irradiation under TEM, the defects on original alumina surface vanished accompanied by the precipitation of nanocrystalline Al particles. By thoroughly analysis of the defect reaction during doping process and the feature of cation sub-lattice of alumina, a defect assisted interstitial atom segregation mechanism was proposed to explain this behavior. According to this mechanism, doped F ions first occupied oxygen vacancy sites with corresponding Al ions at intrinsic interstitial sites. After oxygen vacancies being fully occupied, both F and Al ions tended to settle down at intrinsic octahedron interstitial sites, which resulted in a metastable doping state. Under the act of 1/3 $[1\bar{1}00]$ partial dislocation of alumina matrix, distorted cation sub-lattice generated double aggregated vacant octahedron sites. When these doublets vacant octahedron sites were occupied by foreign Al ions, stacking faults composed of about three sequences were generated as that observed in high resolution TEM. Meanwhile, the segregated doping Al ions at double aggregated octahedron sites along the stacking faults worked as early stage precipitations. Under electron irradiation, with the ablation of F ions, the unstable segregated Al ions separated out as nano precipitation with the reconstruction of alumina lattice.

Key words: AlF_3; Al_2O_3; TEM; electron irradiation; phase-separation

Materials with good irradiation damage tolerance are necessary for modern unclear equipment as core components while those with good irradiation sensitivity can be applied as sensors and detectors for irradiation environment. The study of irradiation effect under various conditions is a prerequisite to screen suitable candidates for both applications. As for the electron irradiation, besides the typical linac irradiation devices, TEM is an alternatively simple and effective method in studying electron irradiation effect, especially for *in-situ* study[1-15].

Alumina is one of the most extensively used structural ceramics and its electron irradiation effects have been well studied. Under conventional TEM observation (accelerate voltage no more than 300 kV, room temperature, and ordinary vacuum of ~10^{-5} Pa) a relative stable nature of alumina was found and only lattice defects like surface faceting[2], stacking fault[3-4] or localized structure degradation[5] were created. When the irradiation condition became critical, decomposition of Al_2O_3 and Al precipitation could be found. Conditions reported for Al precipitating from alumina matrix under TEM observation were relative extreme like high accelerate voltage (above 400 kV)[6-7], high temperature (above 700 K)[6-9], ultra-high dose rate[10-11] or ultra-high vacuum[2]. Bonevich, *et al*[2] reported that metallic Al formed on the surface after 1 h irradiation under ultra-high vacuum

Received date: 2020-11-04; **Revised date:** 2020-02-20; **Published online:** 2020-07-21
Foundation item: National Natural Science Foundation of China (51172248); Zhejiang Provincial Natural Science Foundation of China (R12E020005)
Biography: SHEN Lu(1988–), male, PhD. E-mail: shenlu@nimte.ac.cn
申 璐(1988–), 男, 博士. E-mail: shenlu@nimte.ac.cn
Corresponding author: HUANG Qing, professor. E-mail: huangqing@nimte.ac.cn
黄 庆, 研究员. E-mail: huangqing@nimte.ac.cn

(10^{-8} Pa) while only surface faceting took place under conventional TEM exposure (vacuum of 10^{-5} Pa). Bouchet, *et al*[10] confirmed the reduction of alumina under extremely high dose rate through analyzing the energy loss near edge structure from the EELS results (Electron Energy Loss Spectroscopy, EELS), however, no metallic Al crystals could be directly observed. Until now, the easiest condition for Al fast precipitating from pure alumina under TEM observation was reported by Chen, *et al*[8-9] at temperature above the melting point of Al.

Recently, we reported that transparent alumina ceramic could be easily sintered by SPS with AlF_3 doping[12]. The present study is to reveal the microstructure character of the AlF_3 doped Al_2O_3 by conventional TEM. Interestingly, a novel electron irradiation induced fast phase-separation behavior was observed. Aluminum nano-crystals separated out quickly from original highly defected Al_2O_3 grains, and the grain resulted in well crystallized state after conventional HRTEM observation.

1 Experimental

The 0.1wt% AlF_3 doped alumina ceramic was sintered by SPS with parameters same to our previous report[12]. To obtain a separated grain for TEM observation, ceramic fragments were firstly scratched from the surface of sintered body with a diamond pen. Then the scratched fragments were treated by ultrasonic in ethanol to break the connected boundaries. Finally, the obtained grain suspension was dropt on copper grid for TEM observation. The observation was conducted with two transmission electron microscopes (TEM, JEM2100 and JEM2000F, JEOL, Japan).

2 Results and discussion

Fig. 1(a) is a clean grain surface stripped from surrounding grains by ultrasonic break. The surface was stable under low magnification observation and no attached second phase was observed. However, once the magnification exceeded 200 k magnification, the surface became unstable. Moveable and growing precipitates were emitted from the surface under electron irradiation after several to dozens of seconds. The precipitates were sphere-like separated out at the beginning and generally transformed to faceted shape when lowering magnification or moving observation area. The diameter of these precipitates ranged from 5 to 50 nm. The typical feature of these precipitations displayed in Fig. 1(b). Arrows in Fig. 1(c-d) exhibited the growing of a precipitate accompanied with the decrease of another. The whole process finished within less than 5 s. Moreover, as a general case, when two growing precipitates contacted with each other, instantaneously they coalesced into a whole. The drop-like moving and coalescing behavior indicates a doubtable liquid-like nature of these precipitates. After the spherical-to-faceted transition, lattice fringes were easy to be seen. The 0.235 nm fringe space of the precipitation corresponds to the 0.234 nm-spacing (111) plane of metallic Al (Fig. 1(e)). The precipitates from original alumina matrix were further confirmed to be metallic Al by EELS study of the Al-L_{23} edges of the precipitation layers. In Fig. 2, Each feature peaks are identical with the reference spectrum of Al metal.

Though it was reported that α-alumina is relatively stable under conventional TEM electron irradiation, the decomposition to Al under electron irradiation is a feature of AlF_3 as described in previous studies[13-15]. In

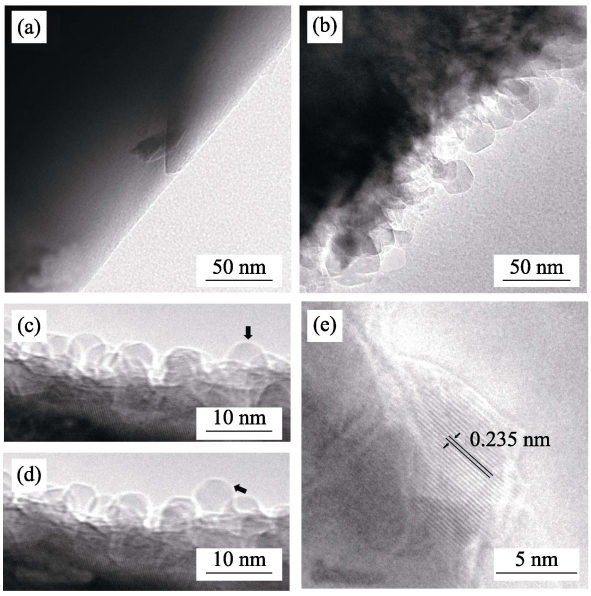

Fig. 1 TEM observations of a grain surface of 0.1wt% AlF_3 doped sample

(a) Original surface before high magnification observation; (b) Surface after high magnification observation, where sphere precipitates separated out; (c-d) Black arrow shows the growing of a new precipitate under irradiation; (e) Lattice fringes of a precipitated crystal

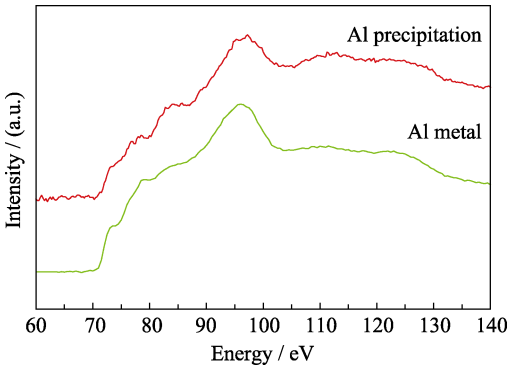

Fig. 2 EELS of the precipitation and its reference

Ghatak, *et al*'s experiment, AlF_3 was not stable under electron exposure and separated into localized 50 nm spherical Al crystals with fast fluorine ablation[15]. The resulted Al crystals are quite similar to the present observed precipitates, thus it is reasonable to conclude that the Al separation under electron irradiation is not the intrinsic property of alumina matrix but an extrinsic feature come from AlF_3 doping. First, the conventional TEM observation only results in lattice defeats in alumina[2-5]. Bonevich, *et al*[2] reported that the original smooth surface became highly faceted under conventional 100 or 300 kV TEM electron irradiation with prolonged observation time. Tomokiyo, *et al*[3] found that planar defects and holes with preferred orientation could be produced near the surfaces under 200 kV TEM observation. Recently, Chen, *et al*[5] found that under HRTEM observation (vacuum lower than 10^{-6} Pa), phase transformation of thermal stable α-alumina to metastable κ' phase occurred under 100 kV electron irradiation. Unfortunately, no Al precipitation was observed in all these studies. Moreover, different from the electron-irradiation-induced lattice defects in alumina[2-3], the present precipitation of Al crystalline resulted in a defect-free state from the original one carried stacking faults, as will be discussed in the following paragraphs. Second, the typical precipitation of Al under critical TEM condition accompanies with holing alumina matrix due to mass transportation[3-4,7-9,11], while it is not the present case since no apparent holing is observed and the surface becomes stable again once after precipitation of Al crystals.

It will be easy to understand this behavior if the AlF_3 was preferentially segregated at the surface. To further understand the phase-separation behavior and make clear the character inside a grain, another HRTEM and selected area diffraction were conducted with JEM-2100F. However, the results shown in Fig. 3(a-d) don't seem to favor this assumption. Fig. 3(a) shows an original grain before irradiation induced Al precipitation. The white arrows point to the dark liner contrasts which suggesting the existence of planer defects. Diffraction pattern of the original grain is shown in Fig. 3(c), where the bright streaks identical with the liner contrasts in Fig. 3(a) confirm the existence of planer defects through the whole grain. It is interesting to note that, once after the Al precipitation by electron irradiation (Fig. 3(b)), the streaks in diffraction pattern of the same grain disappeared (Fig. 3(c)), indicating the precipitation of Al involved the reconstruction of lattice and finally resulted in a defect free state. Fig. 3(e) is the magnification of area i in Fig. 3(a), where the white dotted box traces a burgers circuit of an edge dislocation and the white arrow

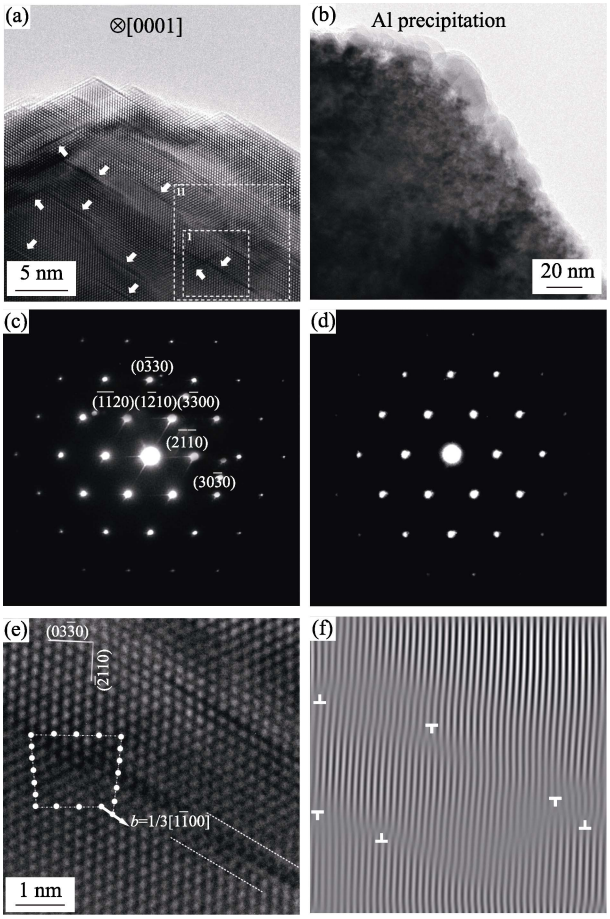

Fig. 3　HRTEM images and selected area diffraction of AlF_3 doped alumina grain

(a) HRTEM images of AlF_3 doped alumina grain before Al precipitation. White arrows points to the planer defects; (b) The same grain after Al precipitation; (c, d) Diffraction patterns correspond to the grain before and after Al precipitation, respectively. The zone axis is along [0001] direction; (e) Magnification of area i in (a). The dotted box traces a dislocation core and the parallel lines show the distortion contrast composed of three or four layers; (f) Inversed FFT of the area ii in (a) from $(2\bar{1}\bar{1}0)/(\bar{2}110)$ diffraction spots

points the Burgers vector. An extra half atom plane can be clearly seen in the center of the box. Fig. 3(f) is the inversed FFT of area (ii) in Fig. 3(a) from $(2\bar{1}\bar{1}0)/(\bar{2}110)$ diffraction spots, where many extra half-planes with dislocation mark can be seen, indicating the highly defected nature.

Two kinds of defects reactions often involve in the doping process, namely substitution-vacancy and interstitial processes. The reaction equation can be written as below in the present case:

$$AlF_3 \xrightarrow{Al_2O_3} Al_{Al} + 3F_O^{\bullet} + V_{Al}''' \quad (1)$$

$$AlF_3 \xrightarrow{Al_2O_3} 3l_F' + l_{Al}^{\bullet\bullet\bullet} \quad (2)$$

Since the Al precipitated without holing the obvious matrix, it is hard to image the vacancy type reaction (1) dominates since the precipitated Al would be otherwise easier to settle down at Al vacancies. On the other hand,

oxide ceramics sintered by SPS often accompanies oxygen vacancies due to the graphite surroundings and chamber vacuum[16-17]. Wang, *et al*[16] reported that excellent green emission caused by oxygen vacancies was observed in SP-sintered ZnO ceramic due to the vacuum ambience. The oxygen vacancies raised during SP-sintering process also resulted in degraded transparency in Y_2O_3 as reported by Jiang, *et al*[17]. Thus, it is reasonable to speculate that the doped F^- ions first occupy oxygen vacancy sites with corresponding Al^{3+} at intrinsic interstitial sites. After oxygen vacancies being fully occupied, both F^- and Al^{3+} tend to settle down at intrinsic interstitial sites as reaction (2). In this case, the settlement of extrinsic doping ions at oxygen vacancies or vacant interstitial sites will block the diffusion path of intrinsic Al^{3+} and O^{2-} ions and inhibit the sintering process, which is quite identical to what we found recently by microstructure evolution analysis——AlF_3 doping working as diffusion inhibitor during the sintering process. However, it is generally unstable for extra F^- anions to settle down at octahedron vacancy sites due to the surrounding electrostatic repulsion. This means that the system may be in metastable state, which is perhaps the root cause of the phase-separation behavior. Moreover, the doping of F^- was supposed to react with carbon contamination and emitted as gas products $(CF)_x$ in previous researches[18-19]. If this reaction exists within the sample, the solid dissolved F^- and Al^{3+} ions may be non-stoichiometric with surplus Al^{3+} ions in alumina matrix.

Considering that the bright streaks in diffraction pattern (Fig. 3(c)) and the corresponding liner contrasts in HRTEM (Fig. 3(a)) are quite similar to the feature of GP zones[20], the liner contrasts may be the segregations of Al atoms or ions in the form of early stage Al precipitates[3-4].

Fig. 4(a) shows an ideal cation lattice diagram of alumina as suggested by Tomokiyo, *et al*[3]. Each circle represents an oxygen octahedron site. The oxygen sub-lattice is omitted to give a clearer illustration of the vacancies. The fluctuation of Al ions along *C* axis is also ignored. One third of the octahedron site remains unoccupied as shown by the open circles. The half-filled circles in $(\bar{2}110)$ plane illustrate the preferential occupation of foreign Al ions, which results in the segregation of Al ions and the corresponding mono-layer planer defects. More specifically, when combining the atomic character revealed in Fig. 3(e) and the real lattice structure, a clearer dislocation assisted mechanism can be proposed. In α-alumina, the $\{1\bar{2}10\}\langle 10\bar{1}0\rangle$ prism plane slip is the secondary slip system beside the primary basal slip system and the $\langle 10\bar{1}0\rangle$ prism plane dislocations are easy to dissociate to three 1/3 $\langle 10\bar{1}0\rangle$ partial dislocations[21-22]. Fig. 4(b) is the real alumina structure under the projection of $[11\bar{2}0]$ direction. The red dotted line includes two oxygen layers and a fluctuated Al layer inside the oxygen octahedrons. This selected Al layer is repainted under [0001] projection in Fig. 4(c). The open circles inside each Al hexagon represent unoccupied octahedron sites. Triangles at the right side indicate the normal stacking sequence A-B-A-B between two Al layers along $[11\bar{2}0]$ direction. The red arrow at the left side represents a Burgers vector of 1/3 $[1\bar{1}00]$ and dotted line in the center shows the slip or distorting plane. Whether after the passage of a movable 1/3 $[1\bar{1}00]$ partial dislocation or distorted by the existence of a Frank partial dislocation with the same Burgers vector, the deformed atomic structure is shown in Fig. 4(d). The act of a 1/3 $[1\bar{1}00]$ partial dislocation finally results in a

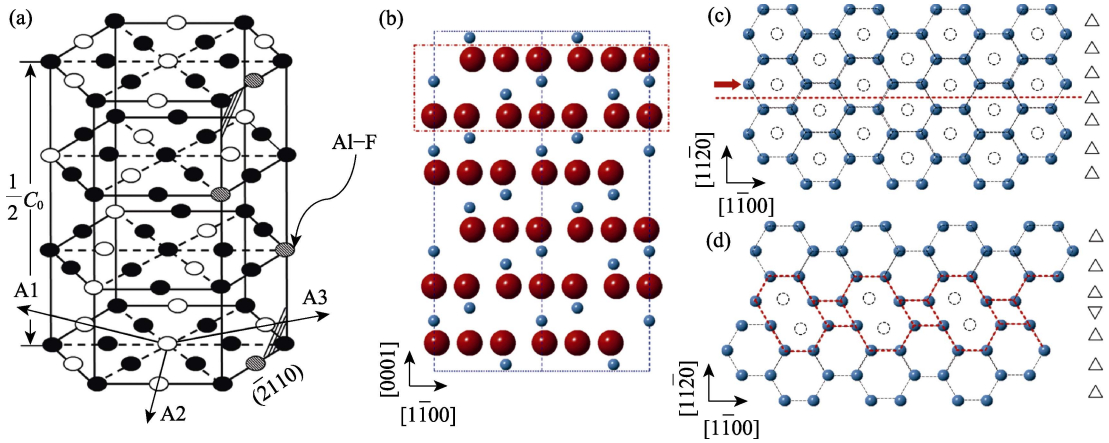

Fig. 4 (a) Schematic diagram of cation sub-lattice in α-alumina. The open and closed circles are the unoccupied and occupied octahedron sites respectively. Half-filled circles represent octahedron sites occupied by extrinsic Al^{3+} ions; (b) Real alumina structure in $[11\bar{2}0]$ projection. The red box selects an Al layer between two oxygen layers; (c, d) Structures of the selected Al ions layer repainted in [0001] projection, before and after the act of a 1/3 $[1\bar{1}00]$ partial dislocation, respectively. The open circles indicate unoccupied octahedron sites in the same layer

stacking fault between the slip plane, and the distorted cation sub-lattice generates a double aggregated vacancy site (Fig. 4(d)). When these doublets vacancies are fully occupied by foreign Al ions, a stacking fault composed of three sequences is generated. This supposed condition is confirmed by the HRTEM in Fig. 3(e), where a distorted contrast composed of three to four layers beside a 1/3 $[1\bar{1}00]$ partial dislocation can be found. As a result, the present defected grain nature can be regarded as planer defects assisted dissolving of AlF_3 into alumina lattice, and in turn, interstitial Al^{3+} ions preferentially segregated at cation vacancies along the stacking faults as early stage precipitations. These segregations are unstable under electron irradiation especially after F^- ablation, and finally separate out as precipitation with the reconstruction of cation lattice.

It is also interesting to note that, LiF has a similar but more sensitive behavior under electron exposure like AlF_3[15]. However, there is no such report so far (to our best knowledge) on the decomposition of LiF doped ceramics (especially for transparent spinels and garnets) under TEM observation even it is quite common for a doping concentration higher than 1%[18-19,23]. This may be due to the intrinsic differences of the defects structure or doping mechanism. Further characterization of LiF doped alumina or AlF_3 doped spinel may be helpful to understand the role of fluoride sintering additives.

3 Conclusions

Until now, we found a novel fast electron-irradiation-induced phase-separation behavior in AlF_3 doped alumina ceramic, which is never reported before. The original grain of the spark plasma sintered sample carried many planer defects with HRTEM observation, Al nano-crystal separated out with these planer defects disappearing. A defects assisted interstitial segregation mechanism was proposed to explain this behavior.

References:

[1] KANEKO K, KATO T, KITAYAMA M, *et al.* Precipitation of $MgO{\bullet}nAl_2O_3$ in Mg-doped α-Al_2O_3 under electron irradiation. *Journal of the American Ceramic Society*, 2003, **86(1):** 161–168.

[2] BONEVICH J E, MARKS L D. Electron radiation damage of α-alumina. *Ultramicroscopy*, 1991, **35(2):** 161–166.

[3] TOMOKIYO Y, MANABE T, KINOSHITA C. Structural change induced near surfaces of α-Al_2O_3 during electron irradiation. *Microscopy Microanalysis Microstructures*, 1993, **4(2/3):** 331–339.

[4] TOMOKIYO Y, KUROIWA T, KINOSHITA C. Defects occurring at or near surfaces in α-Al_2O_3 during electron irradiation. *Ultramicroscopy*, 1991, 39**(1–4):** 213–221.

[5] CHEN C L, ARAKAWA K, LEE J G, *et al.* Electron-irradiation-induced phase transformation in alumina. *Scripta Materialia*, 2010, **63(10):** 1013–1016.

[6] OH S H, KAUFFMANN Y, SCHEU C, *et al.* Ordered liquid aluminum at the interface with sapphire. *Science*, 2005, **310(5748):** 661–663.

[7] PELLS AERE G P, SHIKAMA T. Radiation damage in pure and helium-doped α-Al_2O_3 in the HVEM quantitative aspects of void and aluminium precipitate formation. *Philosophical Magazine A*, 1983, **48(5):** 779–794.

[8] CHEN C L, FURUSHO H, MORI H. *In situ* TEM observation of decomposition of high-purity sapphire. *Philosophical Magazine Letters*, 2009, **89(2):** 113–119.

[9] CHEN C L, FURUSHO H, MORI H. Effects of temperature and electron energy on the electron-irradiation-induced decomposition of sapphire. *Philosophical Magazine Letters*, 2010, **90(10):** 715–721.

[10] BOUCHET D, COLLIEX C. Experimental study of ELNES at grain boundaries in alumina: intergranular radiation damage effects on Al-L23 and OK edges. *Ultramicroscopy*, 2003, **96(2):** 139–152.

[11] BERGER S D, SALISBURY I G, MILNE R H, *et al.* Electron energy-loss spectroscopy studies of nanometre-scale structures in alumina produced by intense electron-beam irradiation. *Philosophical Magazine B*, 1987, **55(3):** 341–358.

[12] WANG D, SHEN L, RAN S, *et al.* Transparent alumina fabricated by SPS sintering with AlF_3 doping. *Scripta Materialia*, 2014, **92(1):** 31–34.

[13] CHEN G S, BOOTHROYD C B, HUMPHREYS C J. Electron-beam induced crystallization transition in self-developing amorphous AlF_3 resists. *Applied Physics Letters*, 1996, **69(2):** 170–172.

[14] MA C, BERTA Y, WANG Z L. Patterned aluminum nanowires produced by electron beam at the surfaces of AlF_3 single crystals. *Solid State Communications*, 2004, **129(10):** 681–685.

[15] GHATAK J, GNANAVEL T, GUAN W, *et al.* Electron Beam Synthesis of 3D Metal Nanostructures from Fluoride Precursors. MRS Online Proceedings Library Archive, 2012**:** 1411.

[16] WANG J, GAO L. Photoluminescence properties of nanocrystalline ZnO ceramics prepared by pressureless sintering and spark plasma sintering. *Journal of the American Ceramic Society*, 2005, **88(6):** 1637–1639.

[17] JIANG D T, MUKHERJEE A K. The influence of oxygen vacancy on the optical transmission of an yttria-magnesia nanocomposite. *Scripta Materialia*, 2011, **64(12):** 1095–1097.

[18] MEIR S, KALABUKHOV S, FROUMIN N, *et al.* Synthesis and densification of transparent magnesium aluminate spinel by SPS processing. *Journal of the American Ceramic Society*, 2009, **92(2):** 358–364.

[19] REIMANIS I, KLEEBE H J. A review on the sintering and microstructure development of transparent spinel ($MgAl_2O_4$). *Journal of the American Ceramic Society*, 2009, **92(7):** 1472–1480.

[20] WILLIAMS D B, CARTER C B. Transmission Electron Microscopy: a Textbook for Materials Science, 2nd edition. New York: Springer Press, 2009**:** 271–282.

[21] HEUER A H, LAGERLOF K P D, CASTAING J. Slip and twinning dislocations in sapphire (α-Al_2O_3). *Philosophical Magazine A*, 1998, **78(3):** 747–763.

[22] CASTILLO-RODRIGUEZ M, MUNOZ A, CASTAING J, *et al.* Basal slip latent hardening by prism plane slip dislocations in sapphire (α-Al_2O_3). *Acta Materialia*, 2010, **58(17):** 5610–5619.

[23] MARDER R, CHAIM R, CHEVALLIER G, *et al.* Effect of 1wt% LiF additive on the densification of nanocrystalline Y_2O_3 ceramics by spark plasma sintering. *Journal of the European Ceramic Society*, 2011, **31(6):** 1057–1066.

AlF_3 掺杂氧化铝陶瓷的高灵敏辐照诱导相分离行为

申 璐[1], 汪德文[2], 黄 荣[3], 都时禹[1], 黄 庆[1]

(1. 中国科学院 宁波材料技术与工程研究所, 宁波 315201; 2. 中国科学院 上海硅酸盐研究所, 上海 200050; 3. 华东师范大学 电子科学系, 极化材料与器件教育部重点实验室, 上海 200062)

摘 要: 放电等离子体烧结的 AlF_3 掺杂氧化铝陶瓷在透射电镜(TEM)常规观察条件下发现了一种电子辐照诱导快速相分离行为。在透射电镜的电子辐照下, 球形纳米晶 Al 颗粒在几秒钟内从原始氧化铝晶粒表面析出。高分辨 TEM 观察结合衍射花样分析发现原始的 F 掺杂氧化铝晶粒表面为高度缺陷态, 电子辐照后, 随着 Al 纳米颗粒析出, 氧化铝晶粒表面的缺陷消失。通过对掺杂过程缺陷反应及氧化铝阳离子亚晶格的深入分析, 提出了一种缺陷辅助间隙原子偏析机理来解释这一现象。即掺杂 F 离子首先占据氧空位的同时 Al 离子占据间隙位, 当氧空位被全部占据时, F 和 Al 离子同时占据基体八面体间隙位, 并形成了亚稳定的掺杂态。在氧化铝基体 1/3 $[1\bar{1}00]$不全位错的作用下, 畸变的阳离子亚晶格产生双聚八面体间隙位。当这些双聚八面体空位被外来 Al 离子占据时, 正如高分辨图像所观察的, 形成了包含有三个原子层左右的堆垛层错。同时, 沿着层错偏聚在双聚八面体位的掺杂 Al 离子扮演了析出物早期的角色, 在电子辐照下随着 F 离子的烧蚀, 不稳定的偏聚 Al 离子析出成为纳米颗粒并伴随着基体氧化铝的晶格重构。

关 键 词: AlF_3; Al_2O_3; TEM; 电子辐照; 相分离

中图分类号: TQ174 **文献标识码:** A